Optics Letters

Three-dimensional particle tracking via tunable color-encoded multiplexing

Martí Duocastella,[1,*] Christian Theriault,[2] and Craig B. Arnold[3]

[1]Nanoscopy, Istituto Italiano di Tecnologia, Via Morego 30, 16011, Italy
[2]TAG Optics Inc., P.O. Box 1572, Princeton, New Jersey 08542, USA
[3]Department of Mechanical and Aerospace Engineering, Princeton University, Princeton, New Jersey 08544, USA
*Corresponding author: marti.duocastella@iit.it

Received 17 November 2015; revised 10 January 2016; accepted 11 January 2016; posted 12 January 2016 (Doc. ID 254075); published 17 February 2016

We present a novel 3D tracking approach capable of locating single particles with nanometric precision over wide axial ranges. Our method uses a fast acousto-optic liquid lens implemented in a bright field microscope to multiplex light based on color into different and selectable focal planes. By separating the red, green, and blue channels from an image captured with a color camera, information from up to three focal planes can be retrieved. Multiplane information from the particle diffraction rings enables precisely locating and tracking individual objects up to an axial range about 5 times larger than conventional single-plane approaches. We apply our method to the 3D visualization of the well-known coffee-stain phenomenon in evaporating water droplets.

OCIS codes: (100.4999) Pattern recognition, target tracking; (170.6900) Three-dimensional microscopy.

http://dx.doi.org/10.1364/OL.41.000863

The rapid 3D tracking of individual particles is crucial in unveiling fundamental processes in diverse fields from fluid mechanics to life science. Despite the development of several optical methods capable of single-particle tracking (SPT) [1], the high-temporal, high-spatial resolution over large volumes required for characterizing the 3D dynamics in important applications such as nanorheology [2] or virus trafficking [3] still remains a challenge. In particular, most microscopy-based approaches can provide nanometer 2D tracking precision, but fail to achieve this precision in the z-direction over extended ranges. Such limitation is mainly due to the loss of signal as the particle moves out of focus. In addition, the axial symmetry of the diffraction spot also impedes proper 3D particle tracking. In other words, the axial distance that the particle moved can be determined by measuring the diameter of its first diffraction ring, provided there is prior knowledge of the particle size [4]; however, such an approach cannot determine whether the particle moved above or below focus. A promising solution to break axial symmetry is to shape the point-spread function (PSF) of the optical system. Successful implementation of this concept includes the use of cylindrical lenses [5] or tailored PSFs, such as a helical PSF [6], in which the shape of the imaged diffraction spot can be unambiguously correlated to the particle axial position. However, these approaches do not alleviate the problem of contrast or signal-to-noise (SNR) loss as the particle moves out of focus, and hence are capable of 3D tracking only in a limited axial range.

A different approach that solves both the problem of out-of-focus loss of SNR as well as axial spot symmetry consists of imaging multiple focal planes quasi-simultaneously [7–10]. The underlying idea of this method is to modify the excitation and/or detection pathways of an optical system to send information from different focal planes into separate cameras or to different sectors of the camera. In this way, the tracking range can be extended and is limited only by the number of planes imaged. Despite the proven feasibility of 3D tracking via biplane imaging, techniques based on this concept suffer different drawbacks. They tend to be difficult to implement; the optical pathway must be divided, and the number of optical elements and cameras makes the setup cumbersome. Furthermore, the SNR is decreased, since light is split between the different detection elements. This is a crucial problem when dealing with small particles whose relatively low emitted signal makes the photon budget a fundamental issue to consider. In addition, these techniques lack flexibility in selecting the image plane locations, due to the fixed position of cameras and optics, which prevent appropriate selection of the region of interest within a sample where 3D tracking is to be performed. Also, when studying dynamic processes in live specimens, sample motion can shift the region of interest with respect to the predefined plane locations. For such applications, one needs methods capable of tunable multiplane selection.

Here, we present what we believe is a novel method for fast 3D particle tracking in bright-field microscopy using multiple and selectable focal planes. Our approach is based on a high-speed electronically tunable lens synchronized with three different monochromatic light sources, each with a different color—red, green, blue (RGB). The driving electronics for the lens enables one to independently control and select the position at which each color is focused. In this way, a single exposure of a color camera will simultaneously capture three colors corresponding to the three different focal planes. By simply splitting the RBG channels, color decoding can be performed and information from up to three different focal planes can be

retrieved [11]. The measurement of the diameter and centroid position of the particle diffraction rings for each of the three focal planes enables one to unambiguously locate and track individual objects over significantly larger axial ranges than conventional single-plane approaches without loss of accuracy. Provided the signal collected from the particles is high enough, the temporal resolution of our 3D tracking approach is only limited by the camera frame rate (fps). Despite the feasibility of an electronic tunable lens for multiplane 3D microscopy having been previously demonstrated [11], an appropriate characterization of the capabilities and potential benefits of this approach for 3D particle tracking have not yet been reported. Note that one can think of the tunable lens to produce a user-controllable chromatic aberration that we use to multiplex illumination and enable multiplane imaging. Although not demonstrated in this Letter, such control of colors could also be used to correct for chromatic aberration. It is also worth noting the parallelism between our method and that based on shaping the PSF; whereas the latter uses shape to encode axial information, we use color. Here, we characterize the tracking accuracy and precision of our approach along the three directions of space, and demonstrate its feasibility by visualizing the fast 3D dynamics of the coffee-stain phenomenon in water droplets.

A schematic representation of our 3D particle tracker is presented in Fig. 1(a). An inverted bright-field microscope is enabled with 3D tracking capabilities by inserting a high speed electronic varifocal lens between the microscope objective (40 × , 0.6 NA) and the tube lens. The position of the varifocal lens close to the objective back focal length assures maximum scanning range and minimal magnification effects [12]. In particular, we use a TAG lens as our varifocal device. This lens uses sound to induce a refractive index gradient in a fluid and, as such, produces a periodic modulation of the focal length in microsecond time scales [13]. For the current experiment, the driving frequency for the standing sound wave is $f_{\mathrm{TAG}} \sim 140$ kHz, and the driving voltage amplitude is 10 V. When combined with a converging lens (i.e., microscope objective), the varifocal capabilities of the TAG lens enable continuous and fast sinusoidal axial scanning [14]. In other words, the axial position of the system focal plane becomes a periodic function of time, with a periodicity of 1/140 kHz ~7 μs. In the experiments presented herein, the total axial scanned range was 10 μm, about an order of magnitude larger than the depth of field (DOF) of the objective used. The z-scanned range decreases with the numerical aperture of the objective, but in general, an axial range of about 10 times the DOF of the objective can be attained when using the TAG lens [11]. Note that this value could be further extended by adjusting the driving amplitude voltage of the TAG lens, with the potential downside of inducing spherical aberration [12]. By using pulsed illumination properly synchronized with the TAG lens oscillation, and provided the light pulses are shorter than the TAG lens oscillation period, any focal plane within the scanning range can be selected. This forms the basis of our approach: we use 300 ns light pulses from three LED sources, each synchronized with a different oscillation state of the TAG lens, and hence a different focal length (the effective focal length of the TAG lens becomes a function of both color and time [see Fig. 1(a)]). In this way, each color can be independently controlled and focused to a user-selectable focal plane within the overall axially scanned range. Indeed, the illuminated planes can be selected by simply changing the temporal phase delay between color pulses and the instantaneous TAG lens focal length. Since each light source has a different color (RGB), the image acquired by the color camera (Infinity 1, Lumenera, pixel size of 4.2 μm) contains information from each plane recorded in each set of color pixels independently. This information can be easily decoded by RGB channel separation. In order to increase contrast, multiple pulses are acquired during the capture of a frame. In fact, the camera is kept at free-running mode while the illumination is pulsed at the frequency of the TAG lens. Thus, the total number of pulses integrated for each captured frame is given by f_{TAG}/fps. In this way, the only synchronization required is between colored pulsed illumination and the TAG lens. Such a scheme greatly simplifies the overall implementation of our approach.

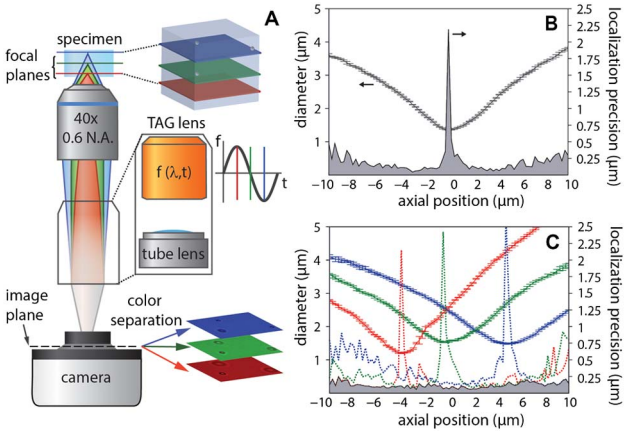

Fig. 1. (a) Schematic of the multiplane imaging setup in which particles are tracked by measuring the diameter and centroid position of the particles first diffraction ring; (b) plot of a 1 μm bead diffraction ring diameter and localization precision versus axial position in a single-plane tracking system; (c) equivalent plot for a three-plane tracking system. The dotted lines correspond to the localization precision for each color/plane, whereas the shadowed area is the global localization precision.

We first determine the axial tracking range of our system by imaging a single bead (1 μm diameter polystyrene sphere) attached to a microscope slide that we translate in the z direction in steps of 250 nm with a piezoelectric stage. At each axial position, we record 25 images for statistical purposes. The average diameter of the bead first diffraction ring versus axial position is presented in Fig. 1(b) for a single focal plane. This plot clearly illustrates the common problem of single-plane-based 3D particle tracking. Notably, the diameter of the diffraction ring is symmetric along the z axis, which limits tracking to a relatively small range either completely above or below focus. In order to better quantify axial tracking range, we calculate the localization uncertainty or localization precision along the z-axis (σ_z) at a certain axial position given the particle diameter ($\varnothing$) and corresponding experimental error ($\Delta\varnothing$) as

$$\sigma_z(z) = \left|\frac{\partial Z(\varnothing)}{\partial \varnothing}\right| \Delta\varnothing(z), \tag{1}$$

where $Z(\varnothing)$ describes the variation of axial position as a function of diameter [Fig. 1(b)]. This equation is simply derived from error propagation. The plot of σ_z versus axial position [gray area, Fig. 1(b)] reveals the increase in uncertainty as one moves closer to focus. This is intuitively expected due to the slow variation of the diffraction ring diameter in the vicinity of the focal plane (±1 μm). In addition, as the bead moves beyond 4 μm above

or below the focal plane, σ_z significantly increases due to a decrease in SNR. Consequently, in this current experiment, traditional single-plane tracking can only provide precise z-information ($\sigma_z < 125$ nm) in a range of about 3 μm.

Contrary to the traditional approach, three-color multiplane imaging obviates most problems that limit the axial tracking range [Fig. 1(c)]. In this case, a unique combination of diameter values exists for each axial position, and hence the axial symmetry of Fig. 1(b) is broken and any potential ambiguity on particle position disappears. In fact, by triangulation, it is possible to uniquely determine the position without prior knowledge of the bead diameter. Most importantly, the deterioration in localization precision close to the focus can be neglected, i.e., one can always identify the z- position from the color channel presenting the lowest σ_z [gray area, Fig. 1(c)]. In this particular experiment, we select three planes located at −5, 0 and 5 μm corresponding to the red, green, and blue colors, respectively. Such conditions enable us to determine the particle z- position with high precision ($\sigma_z < 125$ nm) over a range spanning about 16 μm, an extension by a factor of 5 over the single-plane approach.

The tracking capabilities of our system in the three directions of space are presented in Fig. 2. In this case, we track 1 μm beads contained in a water-filled reservoir while translating it at 250 nm steps in x–y–z at regular intervals of 1.5 s. Considering the frame rate of our camera to be 20 fps, this implies 30 measurements (data values) per xyz position. We use an algorithm based on connected neighboring points—implemented in MATLAB—to perform tracking. In more detail, for each frame and color channel, we use the Hough transform to locate the particles and determine the diameter of their first diffraction ring as well as the corresponding centroid position. By using the calibration curve derived from Fig. 1(c), and using linear interpolation, we can then determine the xyz coordinates of each particle at a given time. In particular, we use information from the three color channels to roughly find the axial position of the particle by error minimization. We then determine the particle axial and lateral position from the color channel that results in the smallest σ. Once the $xyzt$ coordinates of each particle are known, trajectories are reconstructed based on the routine described in [15]. The measured trajectory of a particle stuck on a microscope slide and hence translated at regular time intervals is plotted in Figs. 2(a)–2(c). The sequential 250 nm steps can be easily distinguished for all three directions in a range of 14 μm. In the conditions herein, this value constitutes a true limit only in the z direction, whereas for the x and y direction, it could be extended to the total field of view of the objective (64 and 48 μm, respectively). Since we know the trajectory of the particle, we can use the data acquired to determine tracking accuracy Δ as well as localization precision. To this end, we fit the experimental data to a step function for each direction of space [red line, Fig. 2(a)–2(c)]. Given an xyz position, the localization precision σ for each axis corresponds to the spread of measured values around its mean value, and can be expressed in terms of the standard deviation. The tracking accuracy for each axis can be computed as the deviation of the mean values with respect to the true position of the particle represented by the step function [16]. A summary of the average values obtained along the entire axial range explored, and for each position, are summarized in Table 1. Notably, an average tracking accuracy of 65 nm or better and a localization precision below 55 nm is reached for the three directions of space. Importantly, the accuracy and precision depend primarily on the properties of the elements that constitute the tracker, i.e., piezo-stage precision, camera shot noise, etc., and thus can be further optimized for a given particle size or other experimental characteristics. The TAG lens simply extends the axial range and in fact, experiments with the TAG lens off result in similar tracking performance but over a reduced axial range.

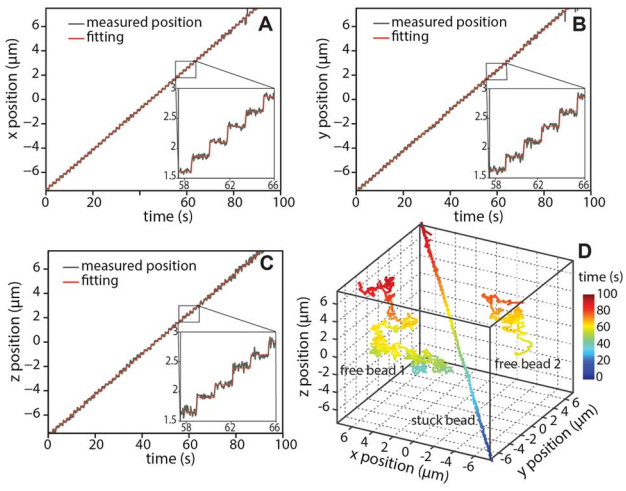

Fig. 2. Characterization of the 3D tracking capabilities of our system. A 1 μm bead stuck on glass is translated in the x, y and z directions at steps of 250 nm, and a tracking algorithm is used to determine the corresponding x, y, z coordinates of the particle at any given time. (a) Evolution of the particle position in the x-axis, (b) y-axis, and (c) z-axis over time. (d) 3D plot of the trajectories of a calibration particle and two freely floating beads.

Although the average values reported are indicative of the performance of our 3D tracker, they do not shed light on the dependence of tracking accuracy and precision along the different positions analyzed. Indeed, one would like to have a method where the overall tracking capability is maintained across the volume analyzed. To this end, the total tracking accuracy and precision at different axial positions is presented in Fig. 3. Note that both parameters present some fluctuations, but no specific trend can be observed over the range analyzed here. Therefore, this experiment demonstrates that our approach enables 3D tracking with an accuracy and precision better than 100 nm across an axial range of 14 μm. Such an extended z-range is in contrast to traditional-single plane approaches, where degradation of accuracy and precision rapidly occurs as one moves away from the plane of interest [4].

The accuracy and precision over a large volume (14 μm× 14 μm × 14 μm) of our approach can be better appreciated in Fig. 2(d), where the total trajectory of the stuck particle is plotted for the three spatial directions. In this case, the trajectories of two free-floating beads have also been included. It is interesting to

Table 1. Tracking Performance of Our System Along an Axial Extent of 14 μm[a]

	x	y	z	Total
Localization precision σ (nm)	40	45	54	80
Tracking accuracy Δ (nm)	25	33	45	61

[a]The total localization precision is calculated as $\sigma_{xyz} = (\sigma_x^2 + \sigma_y^2 + \sigma_z^2)^{1/2}$, the total tracking accuracy as $\Delta_{xyz} = (\Delta_x^2 + \Delta_y^2 + \Delta_z^2)^{1/2}$.

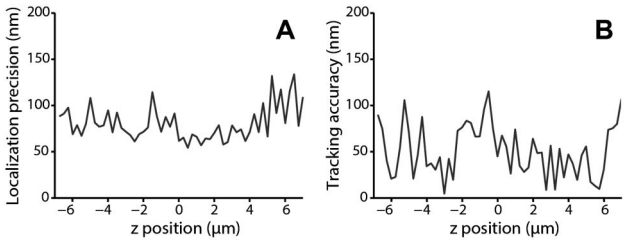

Fig. 3. Plot of the total localization precision (a) and tracking accuracy (b) along the different axial positions over which 3D tracking is performed. The values are computed using 30 data points per position, at the same conditions as described in Fig. 2.

note the difference between the regular movement of the stuck particle, controlled by the piezoelectric translation, and the random walk of the free beads caused by Brownian motion.

Finally, we characterize the dynamics of an evaporating water droplet containing 1 μm beads (0.1% solid concentration) to highlight the speed at which z-positional information can be acquired from a large collection of beads in the same image. The RGB images captured using our particle tracker at a frame rate of 20 Hz and over a time span of 8.25 s are shown in Visualization 1 and Fig. 4. Clearly, each color channel corresponds to a different focal plane as indicated by the different size of the first diffraction ring of a given particle. Note that all images seem to present some motion blur. This is not a limitation of our approach but a limitation of the settings of the experiment. In fact, during the 50 ms exposure time of each frame, the particle's movement cannot be fully discarded. Also, the curvature of the droplet may cause some degradation in image quality. In any case, by using the multiplane information and the tracking algorithm developed here, we can determine the particle trajectories [Fig. 4(d)]. All particles, independent of their initial position, converge toward the edge of the droplet–even particles that were initially at different axial positions. The results obtained and the evolution of the reconstructed 3D trajectories are consistent with the coffee-stain

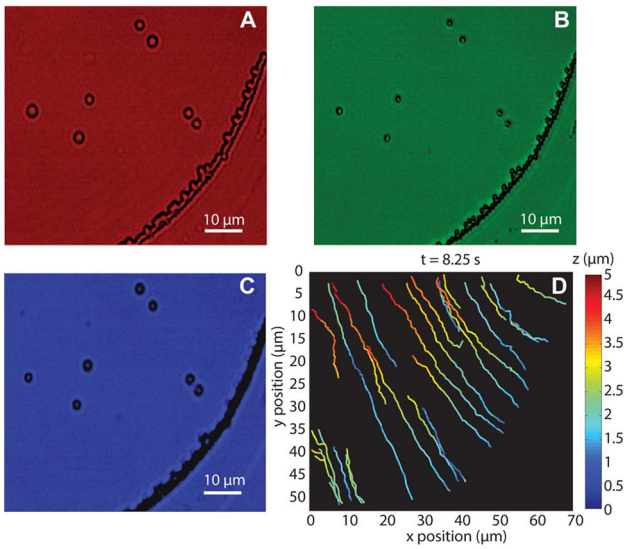

Fig. 4. 3D tracking of 1 μm beads in an evaporating drop of a water. (a)–(c) Snapshot of the RGB channels captured at 8.25 s corresponding to the three different focal planes simultaneously captured; (d) color plot of the particle trajectories from 0 to 8.25 s. See Visualization 1.

phenomenon, a well-known process caused by the pinning of the contact line and the induced capillary flow as a droplet evaporates. Despite extant literature on the study of this inherently 3D phenomenon, most works use 2D tracking approaches [17], which neglect the potential role that axial flow components can play. In contrast, our method enables one to significantly extend the tracking capabilities of a 2D system with the simple introduction of tunable lens, while preserving the tracking speed, localization precision, and tracking accuracy of existing 2D approaches. This is a step forward in the study of 3D processes that require high tracking accuracy and precision over extended axial ranges.

In conclusion, bright-field microscopy with tunable color-encoded illumination is a powerful approach to perform 3D particle tracking over extended ranges with high precision and accuracy. Our simple method, based on a single fast electronic liquid lens known as the TAG lens, offers the possibility of selecting an arbitrary number of different focal planes without moving mechanical elements or, more importantly, sacrificing SNR. With a simple calibration, the unique relationship between particle axial position and RGB diameters can be determined, enabling particle tracking over large volumes. Contrary to other multiplane approaches, color-coded multiplexing can be used with a single detection element, allows full frame capture, and can be directly incorporated in any bright-field imaging system. The simplicity and tunability of our 3D tracker is suitable for characterizing the dynamics of a wide variety of processes spanning different spatial and temporal scales, giving researchers an important new tool capable of exploring 3D phenomena with exceptional detail.

Funding. Division of Materials Research (DMR) (DMR-1420541).

REFERENCES

1. K. Jaqaman, D. Loerke, M. Mettlen, H. Kuwata, S. Grinstein, S. L. Schmid, and G. Danuser, Nat. Methods **5**, 695 (2008).
2. D. Alcor, G. Gouzer, and A. Triller, Eu. J. Neurosci. **30**, 987 (2009).
3. B. Brandenburg and X. Zhuang, Nat. Rev. Microbiol. **5**, 197 (2007).
4. M. Wu, J. W. Roberts, and M. Buckley, Exp. Fluids **38**, 461 (2005).
5. H. P. Kao and S. Verkman, Biophys. J. **67**, 1291 (1994).
6. M. A. Thompson, M. D. Lew, M. Badieirostami, and W. E. Moerner, Nano Lett. **10**, 211 (2010).
7. E. Toprak, H. Balci, B. H. Blehm, and P. R. Selvin, Nano Lett. **7**, 2043 (2007).
8. K. Peterson, B. Regaard, S. Heinemann, and V. Sick, Opt. Express **20**, 9031 (2012).
9. P. A. Dalgarno, H. I. C. Dalgarno, A. Putoud, R. Lambert, L. Paterson, D. C. Logan, D. P. Towers, R. J. Warburton, and A. H. Greenaway, Opt. Express **18**, 877 (2010).
10. S. Ram, P. Prabhat, J. Chao, E. S. Ward, and R. J. Ober, Biophys. J. **95**, 6025 (2008).
11. M. Duocastella, B. Sun, and C. B. Arnold, J. Biomed. Opt. **17**, 050505 (2012).
12. M. Martínez-Corral, P. Y. Hsieh, A. Doblas, E. Sánchez-Ortiga, G. Saavedra, and Y. P. Huang, J. Display Technol. **11**, 913 (2015).
13. A. Mermillod-Blondin, E. McLeod, and C. B. Arnold, Opt. Lett. **33**, 2146 (2008).
14. M. Duocastella, G. Vicidomini, and A. Diaspro, Opt. Express **22**, 19293 (2014).
15. J. C. Crocker and D. G. Grier, J. Colloid Interface Sci. **179**, 298 (1996).
16. H. Deschout, F. Cella Zanacchi, M. Mlodzianoski, A. Diaspro, J. Bewersdorf, S. T. Hess, and K. Braeckmans, Nat. Methods **11**, 253 (2014).
17. T. Kajiya, D. Kaneko, and M. Doi, Langmuir **24**, 12369 (2008).